VIII. MICROWAVE ELECTRONICS*

Prof. L. D. Smullin
Prof. H. A. Haus
A. Bers
P. Chorney
T. J. Fessenden
W. D. Getty
S. Holly
R. Litwin
A. Zacharias

A. NOISE MEASUREMENTS ON ELECTRON BEAMS AT 3000 MC

The noise parameters S and Π/S have been measured (1) for an electron beam produced by a multiple-region electron gun manufactured by Bell Telephone Laboratories, Incorporated. This electron gun is used in a traveling-wave tube that operates in the 3000-mc region. The noise figure obtainable from these tubes is approximately 3 db. In our measurements we attempted to observe two things: (a) agreement between the measured noise figure of the traveling-wave tube and the theoretical minimum obtainable noise figure predicted from our measurements of S and Π/S, and (b) whether the noise parameters can be varied by changing the conditions under which the beam is drawn from the cathode.

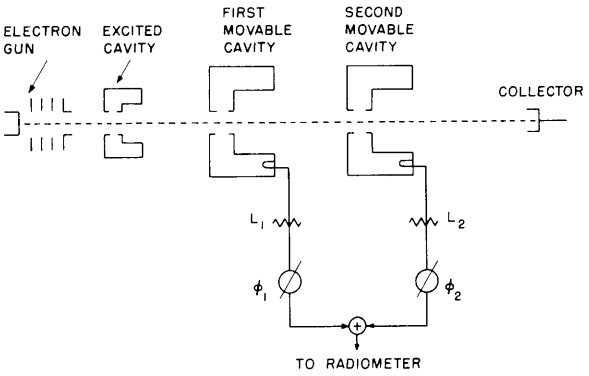

Fig. VIII-1. Beam-noise measuring apparatus.

An unexplained discrepancy in the measurement of the absolute value of the S parameter prevents us from observing the former agreement, but the phenomenon of variation of the noise parameters was definitely established.

Because the measuring apparatus has been described by Saito (2) and by the author (3), only a brief description is given here. Two identical movable cavities are positioned one-quarter space-charge wavelength apart. The output of each cavity is connected to an attenuator and passed through a phase shifter. Then the outputs of the phase shifters are added in a hybrid Tee (Fig. VIII-1).

A normalized series cavity impedance is defined as

$$r = \frac{M^2\left(\frac{R_s}{Q}\right)Q_L}{Z_o} \qquad (1)$$

*This research was supported in part by Purchase Order DDL-B222 with Lincoln Laboratory, which is supported by the Department of the Army, the Department of the Navy, and the Department of the Air Force under Contract AF19(604)-5200 with M. I. T.

where M^2 is the actual gap-coupling coefficient, Q_L is the loaded Q of the cavity, and Z_o, the beam impedance, is expressed by

$$Z_o = \frac{2V_o}{I_o} \frac{\lambda_e}{\lambda_q}$$

By adjusting the phase shifters and attenuators we can find two sets of values that make the output of the hybrid Tee proportional to either the fast wave or the slow wave of the beam excitation. By using an excited cavity (Fig. VIII-1) that has a short gap and a loaded Q that is much lower than the loaded Q of the pick-up cavities, the beam can be driven by "white" noise with equal fast-wave and slow-wave excitation, provided that the amplitude of the excitation is very much greater than the inherent beam noise. In this manner, the directional beam coupler is calibrated for measurement of the ratio of slow-wave to fast-wave amplitude. If this ratio, called A, is measured for the inherent beam noise, then

$$\frac{\Pi}{S} = \frac{\rho^2 + 1}{2\rho} \left(\frac{1 - A}{1 + A} \right) \tag{2}$$

where ρ^2 is the standing-wave ratio of the noise-current modulation (2).

Note that nowhere in this procedure is the actual value of the mean-square current on the beam required. Also, the only parameter of the pick-up cavities that must be known is r. This can be found experimentally. If we consider the two cavities as a klystron amplifier, the maximum available gain can be obtained for identical cavities that are separated by a quarter space-charge wavelength. This value (4) is

$$G = r^2 \tag{3}$$

The conditions for obtaining this gain are: (a) The input cavity is matched to the generator, and (b) the output cavity is matched to the load. In our case, both cavities were matched to 50-ohm lines with less than 1.2 VSWR. Hence, the observed klystron gain should be r^2. The agreement between the measured value of r^2 and the value of r^2 calculated from Eq. 1, with the values measured for R_s/Q and Q_L and calculated for M^2 and Z_o, is quite good; in fact, the discrepancy is below 30 per cent (1 db).

Thus the value obtained for Π/S is a truly independent measurement that requires knowledge only of ratios of the outputs of the pick-up cavities. The measurement of the S parameter requires a knowledge of the cavity output power induced by a given value of beam noise. The value of S can be found (1) for a drifting beam to be

$$S = Z_o(|\psi_{max}| \, |\psi_{min}|)^{1/2} \tag{4}$$

where ψ is the power-density-spectrum amplitude of the current fluctuations on the

beam. The power-density-spectrum amplitude for full shot noise is given as

$$\psi_{SN} = \frac{eI_o}{2\pi} \tag{5}$$

If the factor $(|\psi_{max}|\,|\psi_{min}|)^{1/2}$ in Eq. 4 can be related to ψ_{SN} for the dc beam current I_o, then S can be determined. We determine ψ_{SN} by exciting the cavity with a beam containing either full shot noise or a known fraction of full shot noise, and comparing the resulting output with the output measured for $(|\psi_{max}|\,|\psi_{min}|)^{1/2}$. If the beam for which the value of S is to be measured has a dc current I_o, and if the value $(\overline{|\psi_{max}|}\,\overline{|\psi_{min}|})^{1/2}$, from the foregoing calibration, equals $\alpha\psi_{SN}$, then, by substitution in Eq. 5, we have

$$S = \frac{eV_o}{\pi}\frac{\lambda_e}{\lambda_q}\,\alpha \tag{6}$$

Since we know the value of r for the pick-up cavity, we can determine the value of α by calculation from the measurement of the mean cavity output. We can also determine the value of α by passing a temperature-limited beam through the cavity and measuring the output. We can also intercept a portion of a space-charge-limited beam (assumed to be completely smoothed) and calculate the full-shot-noise current through the cavity (5).

1. Results of Measurements

The gun was first operated at a beam current of 200 μa. Five pairs of values were found for the beam-focusing electrode voltage and first-anode voltage (Fig. VIII-2) that

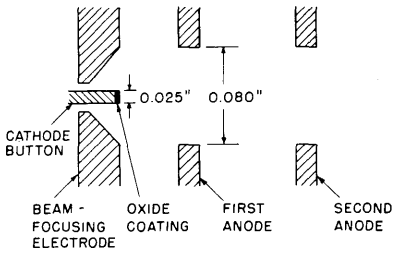

Fig. VIII-2. Bell Telephone Laboratories gun; detail of cathode geometry.

produced low (less than 7 db) standing-wave ratios for the beam-noise current. Measurements of S and Π/S were taken for each of these conditions. The results are tabulated in Table VIII-1. It is seen that the value of S varies over a considerable range. However, the magnitude of S is very large if we consider Haus' (1) relation for the minimum obtainable noise figure for an amplifier with this beam.

$$F_{min} = 1 + \frac{S}{\frac{kT}{2\pi}} \left(1 - \frac{\Pi}{S}\right) \tag{7}$$

for $T = 300^\circ$ K $(kT)/(2\pi) = 0.66 \times 10^{-21}$. The lowest value of $S[1 - \Pi/S]$ that was found would produce a minimum noise figure of 11 db.

The gun was then tested under the operating conditions that produce a 3-db noise figure in the traveling-wave tubes. This was with a beam current of 75 μa and the electrode voltages shown in Table VIII-1. Although the value of S was considerably lower than it was for a beam current of 200 μa, it was still much too high.

Table VIII-1. Values of S Found from Shot-Noise Calibration of First Cavity.

Beam-Focusing Electrode Voltage (volts)	First-Anode Voltage (volts)	Beam Current (μa)	Drift Voltage (volts)	(ρ^2) SWR of Noise Current (db)	S (watt-sec)	$\frac{\Pi}{S}$
+17.0	+ 7.5	200	500	6.0	18.0×10^{-21}	-0.09
+15.0	+10.3	200	500	5.3	15.3×10^{-21}	0.00
+12.0	+18.5	200	500	4.7	9.9×10^{-21}	-0.07
+10.0	+21.5	200	500	3.9	9.7×10^{-21}	+0.13
+ 7.1	+28.2	200	500	3.2	8.4×10^{-21}	+0.06
+10.0	+ 5.4	75	350	2.7	3.8×10^{-21}	+0.16

The method of obtaining the shot-noise calibration was then investigated. Use was made of the North relation for interception noise (5). A 1000-mesh screen was mounted on a rotatable vane. The screen was placed directly in front of the cathode side of the first cavity, and was rotated into the beam. The transmission of the screen was 36 per cent. The power-density spectrum of the noise current passing through the cavity is

$$\psi = \frac{e}{2\pi} I_c \left(\frac{I_k - I_c}{I_k}\right) = \frac{e}{2\pi} I_c (1-t) \tag{8}$$

where I_c is the collector current, I_k is the cathode current, and t is the transmission. The full-shot-noise current passing through the cavity is $I_c(1-t)$. This procedure

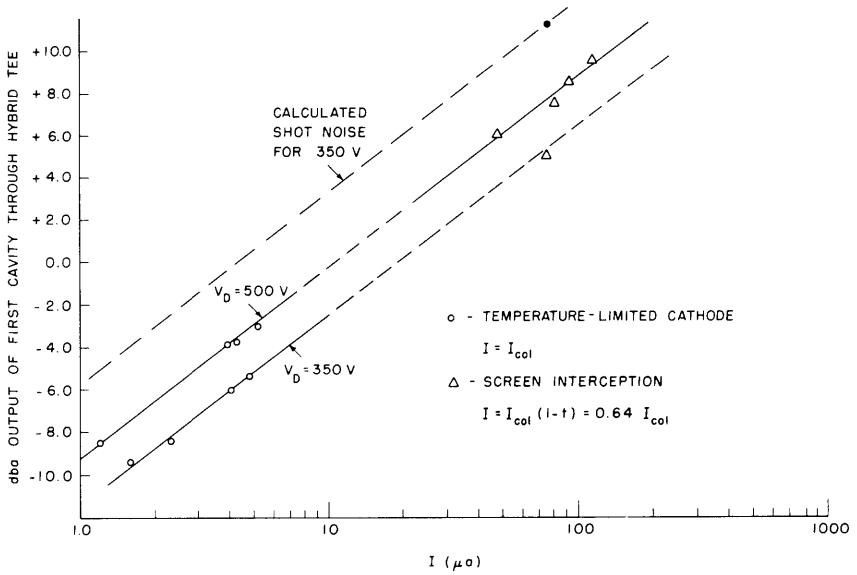

Fig. VIII-3. Measured shot-noise outputs from first cavity.

calibrated the cavity. In checking the calibration we used a temperature-limited beam. The cathode was cooled until less than 10 μa current could be drawn. Then we plotted the cavity output versus collector current (Fig. VIII-3), using drift voltages of 350 volts and 500 volts. On the same plot there is a set of points for interception noise; the abscissa in this case is $I_c(1-t)$. Only one point was taken at 350 volts, but the agreement between the temperature-limited results and the interception results is very good.

The ordinate for these plots requires some explanation. The detector for the measuring system is a radiometer. The presence of beam noise in the cavity gap increases the apparent temperature of the cavity. The radiometer response to this increase, and the ordinate of the graph gives the amount of increase relative to room temperature. Thus, 0.0 dba stands for an apparent increase of cavity temperature that equals ambient temperature of 290° K. The radiometer is calibrated by a gas-discharge noise source with a noise figure of 15 db and a precision attenuator. The radiometer bandwidth is approximately 7.5 mc, and the cavity bandwidth is 6.0 mc, so that the apparent increase in cavity temperature is 1 db higher than the measured apparent increase.

If the cavities are calibrated by using a beam that has a known amount of shot noise, the calibration of the radiometer which has just been discussed is unnecessary. A known value of shot noise in the beam will produce a given radiometer output. All subsequent radiometer outputs can then be referred to this known value of shot noise. For the calculation that will now be discussed, however, the noise source calibration of the radiometer is required.

From a knowledge of r for the cavity, the apparent increase of cavity temperature

caused by full shot noise can be calculated. If the power-density spectrum of the shot noise is ψ with the cavity output matched to the radiometer, we have

$$\psi_o = \frac{1}{2}\psi r Z_o \tag{9}$$

which is the power-density spectrum of the cavity output noise. The power-density spectrum of the cavity noise itself is

$$\psi_{oo} = \frac{kT}{2\pi} \tag{10}$$

where T is ambient temperature, and ψ_{oo} exists independently of the presence of the beam. The ratio of Eq. 9 to Eq. 10 gives the apparent relative increase in noise-power output which results from the presence of a full-shot-noise beam. Hence,

$$\text{dba} = 10 \log \frac{\frac{1}{2}\psi r Z_o}{\frac{kT}{2\pi}} \tag{11}$$

where dba now represents the increase in cavity temperature. By using

$$\psi = \frac{eI_o}{2\pi} \quad \text{and} \quad Z_o = \frac{2V_o}{I_o}\frac{\lambda_e}{\lambda_q} \tag{12}$$

we can find the value of dba. For I_o = 75 μa, V_o = 350 v, and λ_q = 22.5 cm, which are the parameters of the beam for the measurement at the recommended operating conditions, dba = +18.3. Although the hybrid Tee was not required for the S measurement, convenience of connection dictated its use, and thus the cavity power was reduced 3 db. A further reduction of 1 db was made to take into account the difference in bandwidth between cavity and radiometer. When the radiometer is calibrated with the noise source, both sidebands of the receiver are used. The cavity bandwidth allows only one sideband to be used when beam noise is being measured. Thus the increase in radiometer output caused by shot noise will be further reduced 3 db from the value indicated by Eq. 11. Hence,

$$\text{Full-shot-noise output} = 11.3 \text{ dba} \tag{13}$$

However, with the use of the intercepting screen, a reading of only +7.1 dba was obtained for full shot noise at 75 μa.

The observed klystron gain precludes explaining this discrepancy as a reduction in r. Secondary electrons or ions might reduce r by loading the gap electronically, and this would affect the output impedance of the cavity. This was checked by observing the change in the VSWR from the cavity output. No change in VSWR was noted with an unintercepted beam, an intercepted beam, or no beam at all.

If the value of S is calculated by using 11.3 dba as full shot noise for the

75-μa condition, we obtain

$$S = 1.46 \times 10^{-21} \text{ watt-sec} \tag{14}$$

If we use the measured value of Π/S (Fig. VIII-3) for this beam, the minimum attainable noise figure becomes

$$F_{min} = 2.86 = 4.6 \text{ db} \tag{15}$$

With the use of the gun at the 75-μa condition, the BTL traveling-wave tube attains a noise figure of approximately 3 db.

Although the actual values of S are in doubt, by an unknown scale factor, the variation observed with the 200-μa beam, and the major variation observed when we changed to a 75-μa beam, demonstrate clearly the variability of the noise parameters S and Π/S.

A. Zacharias

References

1. H. A. Haus, Analysis of signals and noise in longitudinal electron beams, Technical Report 306, Research Laboratory of Electronics, M. I. T., Aug. 18, 1955.

2. S. Saito, New method of measuring the noise parameters of the electron beam, Technical Report 333, Research Laboratory of Electronics, M. I. T., Aug. 22, 1957.

3. A. Zacharias, Microwave beam measurements, Quarterly Progress Report, Research Laboratory of Electronics, M. I. T., July 15, 1958, p. 45.

4. A. Bers, Experimental and theoretical aspects of noise in microwave tubes, S. M. Thesis, Department of Electrical Engineering, M. I. T., August 1955.

5. D. O. North, Fluctuations in space-charge-limited currents, RCA Rev., Vol. 5, Part III, No. 2 (1940).

B. PLASMA STUDIES

1. ATTENUATION IN ION-LOADED WAVEGUIDES

In the quasi-static, small-signal analysis of plasma waveguides that have circular symmetry and an axially applied dc magnetic field (Fig. VIII-4) we obtain the determinantal equation

$$\beta_z^2 = \frac{\omega^2\left(\omega_p^2 + \omega_c^2 - \omega^2\right)}{\left(\omega_p^2 - \omega^2\right)\left(\omega_c^2 - \omega^2\right)} \beta_r^2 \tag{1}$$

and the boundary matching equation

$$\frac{\omega_p^2 + \omega_c^2 - \omega^2}{\omega_c^2 - \omega^2} \beta_r b \frac{J_1(\beta_r b)}{J_0(\beta_r b)} = -\beta_z b \frac{I_1(\beta_z b) + \frac{I_0(\beta_z a)}{K_0(\beta_z a)} K_1(\beta_z b)}{I_0(\beta_z b) - \frac{I_0(\beta_z a)}{K_0(\beta_z a)} K_0(\beta_z b)} \tag{2}$$

for circularly symmetric modes (1, 2). Here, β_z is the propagation constant, β_r is the radial wave number, ω_p is the plasma frequency, and ω_c is the cyclotron frequency. In

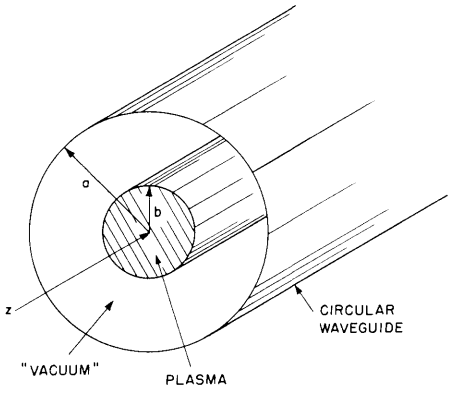

Fig. VIII-4. Plasma-loaded waveguide.

essence, β_r is eliminated from these equations in order to obtain the dispersion relation, β_z, as a function of ω, ω_p, ω_c, a, and b.

Equations 1 and 2 were obtained with collisions ignored. If we now assume that collisions are present and that the collision frequency is a constant, the small-signal force equation can be modified to read

$$j(\omega - j\nu_c)\,\vec{v} = \frac{q}{m}(\vec{E} + \vec{v} \times \vec{B}_o) \tag{3}$$

where $(\nu_c)/(2\pi) = f_c$, the collision frequency. With collisions considered, it is easily shown that in Eqs. 1 and 2, ω becomes $\omega - j\nu_c$, and ω_p^2 becomes $\left(1 - j\frac{\nu_c}{\omega}\right)\omega_p^2$. Hence, we make the same replacements in the dispersion relation and we obtain the modified expression for the complex propagation constant in functional form:

$$\Gamma_z(\omega, \omega_p, \nu_c) = j\beta_z\left(\omega - j\nu_c, \left(1 - j\frac{\nu_c}{\omega}\right)^{1/2} \omega_p\right) \tag{4}$$

where $\Gamma_z(\omega, \omega_p, \nu_c) = \alpha(\omega, \omega_p, \nu_c) + j\beta_z'(\omega, \omega_p)$, in which α is the attenuation constant attributable to collisions, and β_z' is the perturbed propagation constant.

For small-collision frequencies, $\nu_c \ll \omega$, we can expand the right-hand side of Eq. 4 in a Taylor series about (ω, ω_p). Neglecting terms higher than first-order, we obtain

$$\alpha + j\beta_z' = j\beta_z(\omega, \omega_p) + \nu_c \frac{\partial \beta_z}{\partial \omega} + \nu_c \frac{\omega_p}{2\omega} \frac{\partial \beta_z}{\omega_p}$$

and we see that, to first order, the propagation constant is unperturbed and the attenuation constant becomes

$$\alpha = \nu_c \left[\frac{\partial \beta_z}{\partial \omega} + \frac{\omega_p}{2\omega} \frac{\partial \beta_z}{\partial \omega_p} \right] \tag{5}$$

This derivation of the attenuation is patterned after that of Trivelpiece (2). In his analysis, apparently, he neglects the effect of collisions on ω_p^2, and therefore his expression for attenuation consists of only the first term of Eq. 5.

Experimentally, we can measure the attenuation constant α and the propagation constant β_z as functions of ω and ω_p. From these measurements we can calculate the collision frequency by using Eq. 5. For the limiting case of zero dc magnetic field, Eq. 5 reduces to

$$\alpha = \frac{1}{2} \nu_c \frac{\partial \beta_z}{\partial \omega}$$

P. Chorney

References

1. P. Chorney, Electron-stimulated ion oscillations, Technical Report 277, Research Laboratory of Electronics, M. I. T., May 26, 1958.

2. A. W. Trivelpiece, Slow wave propagation in plasma waveguides, Technical Report No. 7, Electron Tube and Microwave Laboratory, California Institute of Technology, May 1958.

2. PRELIMINARY TRANSIENT ANALYSIS OF A PLASMA PRODUCED IN A RESONANT CAVITY BY MICROWAVE ENERGY

The transient build-up of a plasma produced by a high-power pulse of microwave energy in a cylindrical cavity resonant in the TM_{010} mode is being studied. The differential equations of the system will be solved by means of an analog computer.

The following assumptions have been made:

1. The positive ions have an infinite mass compared with that of the electrons.

2. The effects of ion recombination, ion diffusion from the plasma, and ion attachment are negligible.

3. The electric field in the plasma is uniform.

The resonant cavity and power source are represented as a parallel-resonant circuit coupled to a current source by a perfect transformer. The plasma is represented

as a nonlinear admittance that loads the resonant circuit (see Fig. VIII-5).

The node voltage equation of the circuit is

$$\frac{I(t)}{K} - J(t) = \left[\frac{1}{R} + \frac{1}{R_o K^2}\right] V(t) + \frac{\omega Q}{R}\int_0^t V(t)\,dt + \frac{Q}{R\omega}\frac{dV(t)}{dt} \tag{1}$$

where J(t) represents the current through the nonlinear admittance, which corresponds to the plasma current. This equation is not suitable for an analog-computer solution because for large Q the integral term and the differential term are quite large even

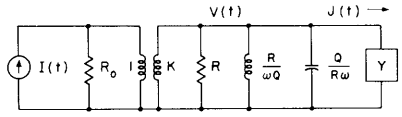

Fig. VIII-5. Circuit model for cavity and plasma with source.

though their sum is small. This trouble can be avoided by a suitable change of variables in the frequency domain.

Solving for V(s) in the frequency domain, we have

$$V(s) = \frac{R\left[\frac{I(s)}{K} - J(s)\right]}{\left[\left(1 + \frac{R}{R_o K^2}\right) + \frac{Q}{\omega}\left(\frac{s^2 + \omega^2}{s}\right)\right]} \tag{2}$$

If we let $\lambda = (s^2 + \omega^2)/s$, Eq. 2 becomes

$$V(\lambda) = \frac{R\left[\frac{I(\lambda)}{K} - J(\lambda)\right]}{\left[\left(1 + \frac{R}{R_o K^2}\right) + \frac{Q}{\omega}\lambda\right]} \tag{3}$$

Converting Eq. 3 to a new time domain τ, we obtain

$$\frac{Q}{\omega}\frac{dV(\tau)}{d\tau} + \left(1 + \frac{R}{R_o K^2}\right) V(\tau) = R\left[\frac{I(\tau)}{K} - J(\tau)\right] \tag{4}$$

It is seen that if V(t) is of the form A(t) cos ωt, then V(τ) is equal to A(t). The source current I(t) = I cos ωt becomes simply I. Thus the substitution mentioned above removes the sinusoidal frequency variation from the variables.

The plasma current is found from the equation

$$J(t) = e \int_A N(t)\ \nu(t)\ da \approx e\, N(t)\ \nu(t)\, A \tag{5}$$

where N(t) is the number of ions per unit volume, $\nu(t)$ is the electron velocity, A is the area of the plasma cross section, and e is the electronic charge.

The electron velocity is obtained from the equation

$$\frac{d\,\nu(t)}{dt} + T_m\, \nu(t) = -\frac{e}{m}\, E(t) = +\frac{e}{m}\, \frac{V(t)}{d} \tag{6}$$

where T_m is the collision frequency, E(t) is the electric-field intensity, and d is the length of the plasma discharge. At practical plasma pressures it is found that the contribution arising from the term $T_m\, \nu(t)$ is negligible and can be neglected. This equation can now be solved for the peak electron velocity, $\nu(\tau)$.

$$\nu(\tau) = \frac{e}{m}\, \frac{V(t)}{\omega d} \tag{7}$$

The electron density is found (2, 3) from the equation

$$\frac{d\,N(t)}{dt} = a_i(t)\ N(t)\ \left|\nu(t)\right| \approx a_i(t)\ N(t)\ \overline{\nu(t)}^{\,t} \tag{8}$$

where $a_i(t)$ is the first Townsend ionization coefficient, and is a function of the electric-field intensity. [$a_i(t)$ is given in the form of a graph by Brown and Allis (3).]

In the τ domain Eq. 8 becomes

$$\frac{d\,N(\tau)}{d\tau} = a_i(\tau)\ N(\tau)\ \frac{\nu(\tau)}{\sqrt{2}} \tag{9}$$

Equations 4, 5, 7, and 9 are to be solved by the computer. These equations are easily programmed for an analog-computer solution (4). This problem is being solved on the analog computer facilities located in the Servomechanisms Research Laboratory, M. I. T.

T. J. Fessenden

References

1. S. C. Brown, High frequency gas-discharge breakdown, Technical Report 301, Research Laboratory of Electronics, M. I. T., July 25, 1955.

2. J. D. Cobine, Gaseous Conductors (Dover Publications, Inc., New York, 1941).

3. S. C. Brown and W. P. Allis, Basic data of electrical discharges, Technical Report 283, Fourth Edition, Research Laboratory of Electronics, M. I. T., June 9, 1958.

4. REAC Analog Computer: Theory and Operations Manual, Report 6080-1, prepared by Department of Electrical Engineering and D. I. C. Staff Members, M. I. T., March 15, 1954.

C. MEASUREMENTS OF THE PHASE CONSTANTS OF THE SHIELDED HELIX

In continuing the work (1) described in Quarterly Progress Report No. 52, measurements of the phase constant and the phase velocity of the slow wave of a shielded helix were made. The same traveling-wave-tube helix was placed inside a metal tube and was soldered to the discs that close the tube at both ends. Such a structure can be considered a section of a short-circuited transmission line. The measurements were made by using essentially the same method and equipment that were previously described. The phase constant β was computed from the formula

$$\beta = \frac{2\pi}{\lambda_z} = \frac{\pi n_1}{\ell_1}$$

where λ_z is the wavelength along the axis of the helix, ℓ_1 is the length of the line, and n_1 is the resonance number – that is, the number of half-wavelengths along the axis of the line. At the lower frequencies the resonance numbers were determined by observing the changes of the resonant output caused by perturbation of the field by means of screws placed at suitable intervals along the tube. In order to distinguish the slow-wave resonances of successive numbers from the resonances corresponding to the other modes at higher frequencies, the field in the vicinity of the helix was perturbed by a plunger that was moved perpendicularly to the axis of the helix through a hole placed exactly at the center of the tube length. This point occurs at the maxima of the electric fields at the resonances of odd numbers and at the maxima of the magnetic fields at the resonances of even numbers. As a consequence, the changes of the resonant frequency resulting from the perturbations at the even- and odd-number resonances occur in opposite directions. The field distribution, and consequently the rate of detuning of the resonances of closest numbers, varies in a regular manner as the number of the resonance. This method enables us to distinguish them from all others. It is most sensitive if the generator that feeds the cavity is not tuned exactly to the resonance but to a frequency on the slope of the resonance curve. Of course, the use of a sweep generator and a panoramic indicator makes measurement easier. Successive resonances of numbers up to 75, where the value of ka is near 0.7, were measured. ($k = (2\pi f)/c$ is the phase constant of the wave in free space, and a is the mean radius of the helix.) At still higher frequencies, resonances are very close to each other and sometimes overlap, or are so strongly coupled that several of them appear as a single resonance. The situation in this region is explained by Fig. VIII-6 [cf., Pierce and Tien (2)], which shows the behavior of the lower components of a shielded helix. The lowest components of the slow wave (m = 0 and m = 1, in Pierce's notation), as a result of coupling to the m = -2 and m = 1 components of the slow wave and to the components of the H_{11} mode, change their slope and, finally, the direction of propagation. In this region, small

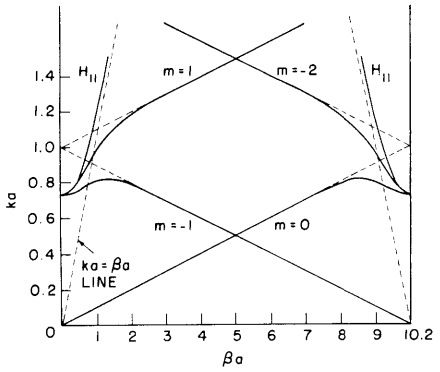

Fig. VIII-6. Lower components of shielded-helix waves.

changes in frequency cause fast changes of the phase constant and of the wavelength, and hence cause a condensation of resonances. Similar behavior of the slow wave in a shielded helix was predicted by L. Stark (3) on the basis of the tape-helix theory introduced by Sensiper (4). Figure VIII-7 shows the experimental results. The dotted and dashed line is the curve of the normalized phase constant versus frequency of the slow wave of a shielded helix. For comparison, the thick solid line shows part of a similar curve of the open helix. The thin solid line is the computed ka-versus-βa line for the nondispersive case. The curves of the normalized phase constant, or normalized phase velocity, for both helices are shown in other coordinates in Fig. VIII-8. With the shielded helix, as predicted by the theory, smaller dispersion in the lower frequency regions can be observed. This is the result of the suppression, by the metal tube, of the field that extends radially from the helix. From the comparison of both curves with the theoretical line we can compute the effective radii of both helices. With the open helix, the ratio of the effective to the mean radius of the helix

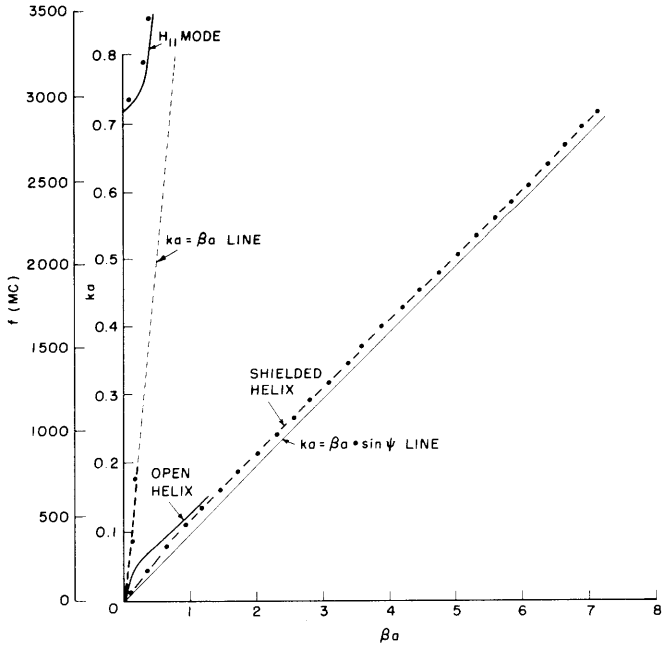

Fig. VIII-7. Measured helix waves.

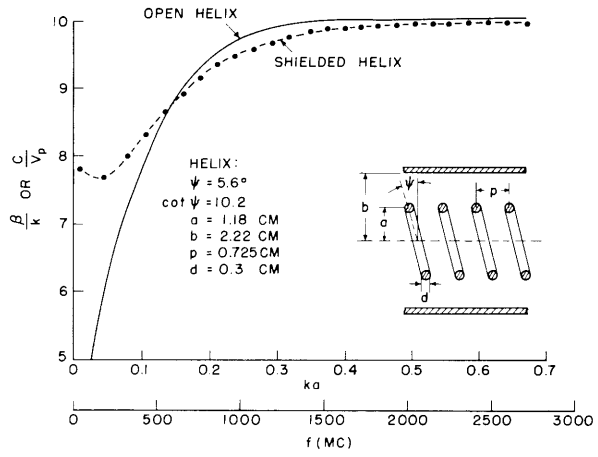

Fig. VIII-8. Comparison of dispersion curves of open and shielded helices.

is $(a_{eft})/a \approx 0.99$, and with the shielded helix, it is somewhat smaller, being 0.97.

From the theory of wave propagation along helical lines, we know that the slow wave guided by the helix is reflected by a conducting plane perpendicular to the axis of the helix in such a manner that the reflected wave tends to spiral in the direction opposite the forward wave. This could introduce some end effects in a short-circuited helix line and could thus reduce the accuracy of the measurements. However, comparison of the results of the measurements on short-circuited helices of different lengths shows no differences, and so these end effects seem to be negligible. The probable explanation is that an opposite-rotating wave, being very strongly attenuated, does not satisfy the boundary conditions on the surface of the helix. The currents induced in the helix by reflected waves tend to flow along the wire and build up the regular helical wave.

1. Fast Waves

Analyses of the shielded helix predict fast waves, $v \geq c$, that correspond to the higher modes of a uniform coaxial cable. These are highpass modes with cutoff frequencies related to the mean circumference of the annular space. Many experimenters have observed peculiar propagation along helices, and this has been vaguely attributed to unidentified fast-modes. In our experiment, we also found a branch (shown by two points on the $\beta a = ka$ line, Fig. VIII-7) with $v/c \approx 1$. One of these resonances did not appear as a separate resonance but, occurring at the same frequency as one of the slow-wave resonances, expanded its amplitude and reduced its Q-value.

The curve H_{11} in Fig. VIII-7 was computed as the lowest waveguide mode in a coaxial line with the radius of the inner conductor equal to the mean radius of the

helix. A few of the lower resonances of this mode, shown as points near this curve, were identified.

R. Litwin

References

1. R. Litwin, Measurements of the phase constant of the slow wave of a helix with the use of the resonance method, Quarterly Progress Report No. 52, Research Laboratory of Electronics, M. I. T., Jan. 15, 1959, p. 49.

2. J. R. Pierce and P. K. Tien, Coupling of modes in helices, Proc. IRE 42, 1389 (1954).

3. L. Stark, The lower modes of a concentric line having a helical inner conductor, Technical Report 26, Lincoln Laboratory, M. I. T., July 2, 1953.

4. S. Sensiper, Electromagnetic wave propagation on helical conductors, Sc. D. Thesis, Department of Electrical Engineering, M. I. T., 1951.